

## Effects of Different Configurations of the East Asian Subtropical and Polar Front Jets on Precipitation during the Mei-Yu Season

LI LI AND YAOCUN ZHANG

*School of Atmospheric Sciences, Nanjing University, Nanjing, China*

(Manuscript received 3 January 2014, in final form 15 May 2014)

### ABSTRACT


Observational analysis indicates that the East Asian jet stream consists of two separate branches: the East Asian subtropical jet (EASJ) and the East Asian polar front jet (EAPJ). The impacts of different intensity configurations of the EASJ and EAPJ on precipitation during the mei-yu season are investigated using the NCEP–NCAR Reanalysis Project (NNRP) dataset and daily gauge observations in East China. The intensity and location of precipitation are associated with different configurations of the EASJ and EAPJ. Precipitation intensity increases with intensification of the EASJ and EAPJ. The rainband is located to the north of the mei-yu region when the EASJ intensifies and the EAPJ weakens. Further analyses indicate that the intensity changes of the EASJ and EAPJ are linked to the cold and warm air mass activities. For cases with strong EASJ and EAPJ, both the warm-moist and cold air masses are active. When the warm-moist and cold air masses meet near 30°N, abundant precipitation occurs in the Yangtze-Huai River basin (YHRB). For cases with weak EASJ and EAPJ, both the cold and warm-moist air masses are inactive, and no significant precipitation occurs in the YHRB. For cases with strong EASJ and weak EAPJ, the warm-moist air mass moves northward while the cold air mass is weak. Precipitation concentrates to the north of YHRB. For cases with weak EASJ and strong EAPJ, cold air extends farther south while the warm-moist air mass is inactive. Precipitation occurs to the south of YHRB.

### 1. Introduction

East Asia is under the strong influence of the summer monsoon. The intense monsoon precipitation that occurs in early summer is known as “mei-yu” in China, “baiu” in Japan, and “changma” in the Koreas (Tao and Chen 1987). The mei-yu precipitation usually accounts for more than 20% of the annual precipitation and sometimes exceeds 50% in the Yangtze-Huai River basin (YHRB; 28°–34°N, 110°–122°E; Wang et al. 2005), which is the most densely populated region in China. While the mei-yu precipitation is a vital water resource for this region, anomalies in mei-yu precipitation especially anomalies in precipitation intensity and rainband location can lead to catastrophic floods and/or droughts in the YHRB (Chen and Chang 1980; Lau

et al. 1988; Ding 1992; Chang 2004; Zhou et al. 2009). The study of mei-yu precipitation is important for disaster prevention and water resource management in the YHRB.

During the mei-yu season, large-scale atmospheric circulation is characterized by distinct features. In the upper troposphere, the strong westerly flow is located around 37°N while in the midtroposphere, the western Pacific subtropical high (WPSH) extends westward to reach the continent with the WPSH ridge line remaining at 20°–25°N steadily. In the lower troposphere at 850 hPa, the warm and moist southwesterly flows originated from the Indo-China Peninsula, from the South China Sea, and from the western Pacific Ocean are dominant over East China (Huang et al. 2011). These synoptic systems have important influences on the mei-yu precipitation. Numerous studies in the literature have described the impact of synoptic circulations in the mid-to lower troposphere on the mei-yu precipitation (Akiyama 1973; Chen and Yu 1988; Kodama 1992). In the upper troposphere, the East Asian jet system is an important circulation system, which acts as a bridge for the eastward propagation of upstream signals (Hoskins and Ambrizzi 1993; Ambrizzi et al. 1995; Lu et al.

 Denotes Open Access content.

*Corresponding author address:* Zhang Yaocun, School of Atmospheric Sciences, Nanjing University, 22 Hankou Rd., Nanjing 210093, China.  
E-mail: yczhang@nju.edu.cn

DOI: 10.1175/JCLI-D-14-00021.1

2002; Enomoto 2004; Ding and Wang 2005; Yasui and Watanabe 2010; Chen et al. 2013) and imposes strong influence on the weather and climate over East Asia (Gong et al. 2001; Yang et al. 2002; Gong and Ho 2003). Changes and variations in the East Asian jet stream provide valuable guidance for the weather and climate predictions.

According to the observational data analyses, the East Asian jet system consists of two separate branches: the East Asian subtropical jet (EASJ) and the East Asian polar front jet (EAPJ). The EASJ is strong and steady, while the EAPJ has significant transient characteristics (Lee and Kim 2003). Most previous studies have focused on the relationship between the EASJ and mei-yu precipitation. The beginning of the mei-yu season is characterized by an abrupt northward jump of the EASJ from 32°N to north of 35°N (Ye et al. 1958; Li et al. 2004), while the abrupt northward jump of EASJ from 40°N to north of 45°N marks the end of the mei-yu (Ninomiya and Muraki 1986; Lin and Lu 2008). The meridional position of the EASJ is closely related to the mei-yu precipitation pattern (Lau et al. 2000; Lu 2004; Kuang and Zhang 2006; Xuan et al. 2011). The location of EASJ core shows distinct zonal variation during the mei-yu season (Zhang et al. 2006; Du et al. 2008). The environmental forcing by the EASJ plays an important role in the formation and maintenance of the mei-yu rain belt (Sampe and Xie 2010; Zhang and Zhou 2012). Although less attention has been paid to the EAPJ, it is found that the seasonal evolution of EAPJ is also linked with the East Asian summer monsoon (Zhang et al. 2008). The seasonal variations in EASJ and EAPJ are both closely related to the mei-yu precipitation.

Recently, more high-resolution data are available for studies to investigate the seasonal variation in the EAPJ and describe precisely the jet core positions. The geographical border between the EASJ and EAPJ becomes clear (Ren et al. 2010, 2011). Some studies discuss the weather and climate episodes from the point of view of concurrent variations between the EASJ and EAPJ. Both climatological studies and single case investigations have revealed that the concurrent variations between the EASJ and EAPJ have a significant impact on the East Asian winter weather and climate (Zhang and Xiao 2013; Liao and Zhang 2013). While the above studies are limited to winter, the relationship among the concurrent variations of the EASJ and EAPJ, the East Asian summer circulation systems, and the mei-yu precipitation still remains unclear. In this study, we attempt to examine the effects of different configurations of the EASJ and EAPJ on the precipitation intensity and spatial pattern during the mei-yu season in summer.

The paper is organized as follows. Section 2 provides a brief introduction of the data used in this study. Section 3 describes the key areas for the EASJ and EAPJ. The precipitation features associated with different configurations of the EASJ and EAPJ are illustrated in section 4. Section 5 shows the associated circulation distributions. The activities of warm-moist and cold air masses with different configurations of EASJ and EAPJ are shown in section 6. Conclusions are given in the final section.

## 2. Data

The daily zonal and meridional wind, temperature, geopotential height, and specific humidity are extracted from the National Centers for Environmental Prediction–National Center for Atmospheric Research (NCEP–NCAR) Reanalysis Project (NNRP) for the time period 1960–2009 (Kalnay et al. 1996). The NNRP is a gridded dataset with  $2.5^\circ \times 2.5^\circ$  horizontal resolution and 17 pressure levels in the vertical. The precipitation observations at 738 stations over the same period provided by the National Meteorological Information Center of China are also used in this study.

The starting and ending dates of the mei-yu season show significant interannual variability. The climatologically mean mei-yu season in China starts after pentad 34 and ends after pentad 38. Hence, we choose the time period from 20 June to 10 July as the climatological mei-yu season.

The statistic calculation of jet center occurrence numbers is performed over the region of 20°–75°N, 60°–160°E. If one specific point satisfies the following conditions: 1) the wind speed is larger than  $25 \text{ m s}^{-1}$  and 2) the wind speed at the eight adjacent grid points surrounding this specific point is less than that at this point, then the location of this point is identified as a jet center.

## 3. Key areas for the EASJ and EAPJ

To characterize the jet intensity changes, two separate key areas are defined for the EASJ and EAPJ, respectively. The jet intensity indices are calculated according to the wind speed over the key areas. Figure 1 shows the latitude–time cross section of 300-hPa wind averaged along 80°–140°E. It is clear that there exist two regions with large wind speed during the mei-yu season: one is located at 37°N and the other is situated at around 65°–70°N. They correspond to the locations of the EASJ and EAPJ, respectively. The average wind speed and jet center occurrence numbers at 300 hPa during the mei-yu season are given in Fig. 2. Based on wind speed and jet center occurrence numbers, two regions over 35°–40°N,

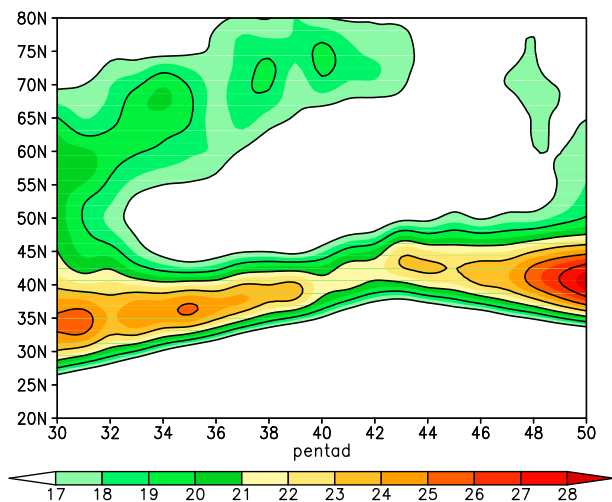


FIG. 1. Latitude–time cross section of the 300-hPa wind averaged along 80°–140°E.

100°–140°E and 62.5°–72.5°N, 80°–140°E are identified as the key areas for EASJ and EAPJ, respectively. The daily area average wind speeds at 300 hPa over the key areas are defined as the daily intensity indices for EASJ (index SJ) and EAPJ (index PJ). Since the wind speed of the EASJ is much larger than that of EAPJ, the standardized index PJ and index SJ are used to evaluate the intensity and variation of the jets by the same standard. Index PJ and index SJ used hereafter are standardized values.

#### 4. Effects of different configurations of the EASJ and EAPJ on precipitation

The features of the mei-yu are characterized by precipitation intensity and spatial distribution. Here we

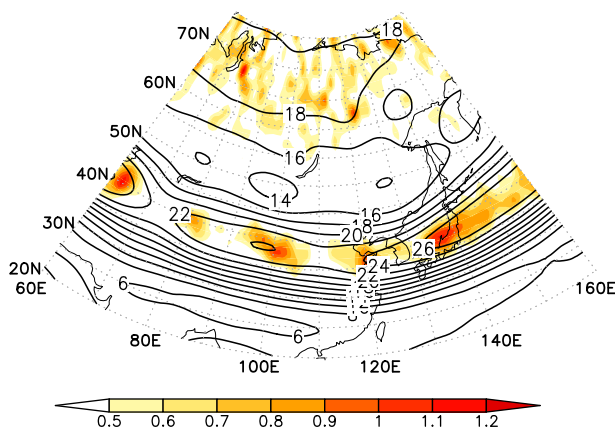


FIG. 2. Spatial distributions of wind (contour) and jet center occurrence numbers (shaded) at 300 hPa during the mei-yu season.

analyze the effect of different configurations of the two jets on mei-yu precipitation intensity and rainband location in the YHRB. Mei-yu precipitation intensity in the YHRB is the average precipitation intensity of all stations in YHRB. Mei-yu rainband location is identified as the average latitude of rainy stations in YHRB. First, the individual variations of the EASJ and EAPJ and their impact on the mei-yu precipitation are investigated. Figure 3 presents the daily precipitation intensity in YHRB versus individual variations of the EASJ and EAPJ intensities. The correlation coefficient between precipitation intensity and index SJ (index PJ) is 0.32 (0.28), which is significant at 5% confidence level. It reveals that the precipitation intensity increases with intensification of the EASJ and EAPJ. Figure 4 shows the daily rainband location in YHRB versus individual variations of the EASJ and EAPJ intensities. The

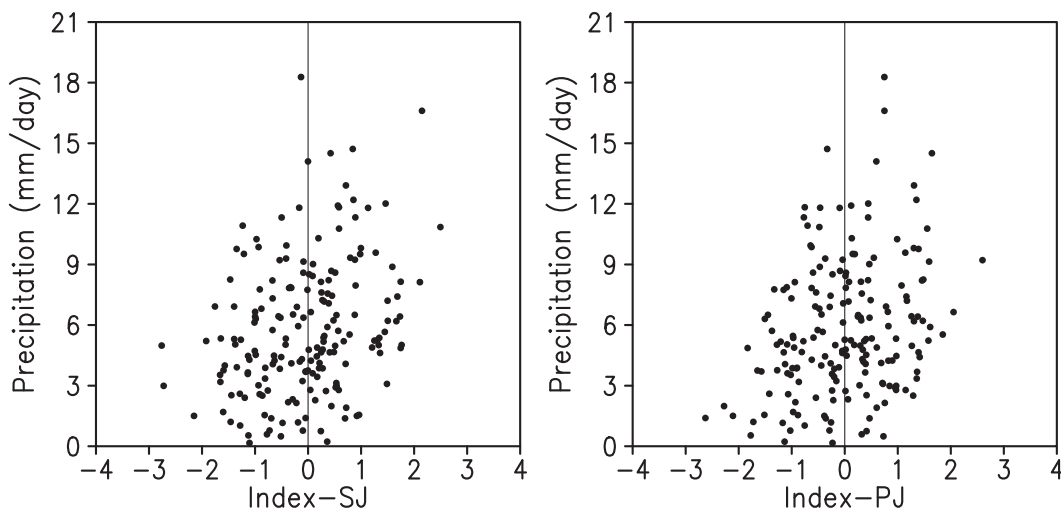


FIG. 3. Daily precipitation intensity changes in YHRB with index-SJ and index-PJ variation.

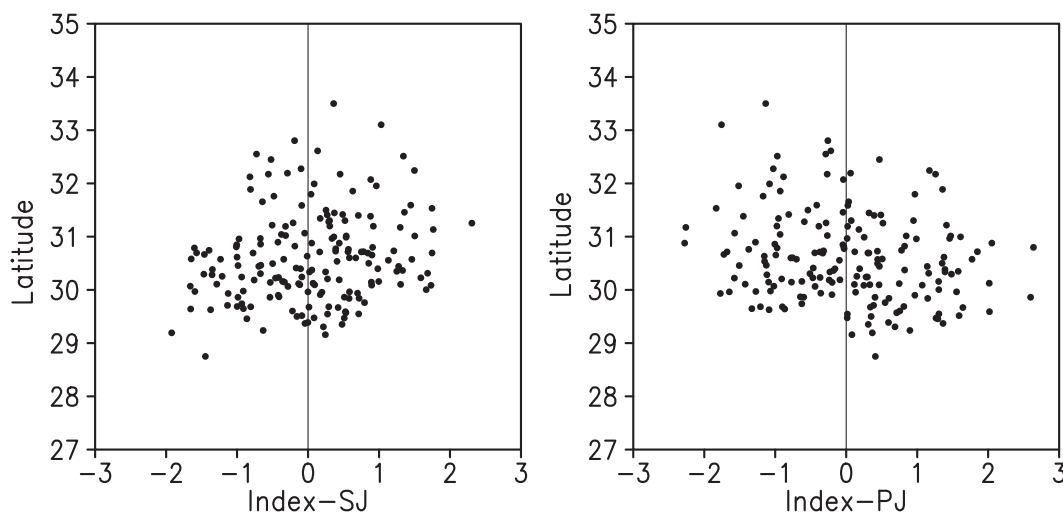


FIG. 4. Daily precipitation area changes in YHRB with index-SJ and index-PJ variation.

correlation coefficient between rainband location and index SJ (index PJ) is 0.20 ( $-0.21$ ), significant at the 5% confidence level. It is found that the mei-yu rainband tends to shift northward when the EASJ intensifies but the EAPJ weakens.

Since the EASJ and EAPJ both belong to the East Asian jet system, and the independent variation of EASJ or EAPJ has effect on mei-yu precipitation, different combinations of their configurations may have various influences on mei-yu precipitation. Here we analyze the effects of concurrent variation of the EASJ and EAPJ on mei-yu precipitation. Based on various intensities of the EASJ and EAPJ, four situations are identified as follows: 1) a strong EASJ accompanying a strong EAPJ (index  $SJ \geq 0.5$  and index  $PJ \geq 0.5$ , SS); 2) a strong EASJ accompanying a weak EAPJ (index  $SJ \geq 0.5$  and index  $PJ \leq -0.5$ , SW); 3) a weak EASJ accompanying a strong EAPJ (index  $SJ \leq -0.5$  and index  $PJ \geq 0.5$ , WS); and 4) a weak EASJ accompanying a weak EAPJ (index  $SJ \leq -0.5$  and index  $PJ \leq -0.5$ , WW). There are a total number of 113, 93, 88, and 136 days corresponding to the above four situations separately during the period 1960–2009.

Spatial distributions of daily precipitation in East China under the above four situations of the EASJ and EAPJ configurations are presented in Fig. 5. For the SS situation, abundant precipitation occurs over the central YHRB. The maximum precipitation occurs along the Yangtze River Valley, and the precipitation rate exceeds  $15 \text{ mm day}^{-1}$  (Fig. 5a). For the SW situation, precipitation is concentrated in the northern YHRB, and the maximum precipitation rate is over  $13 \text{ mm day}^{-1}$  (Fig. 5b). For the WS, precipitation that exceeds  $11 \text{ mm day}^{-1}$  mainly appears in southern YHRB (Fig.

5c). For WW cases, precipitation is concentrated in southern China and little precipitation occurs in the YHRB (Fig. 5d).

## 5. Circulation patterns with different configurations of the EASJ and EAPJ

Circulations with different configurations of the EASJ and EAPJ are examined in this section. Low-latitude circulation systems and mid- to high-latitude circulation systems both have significant impacts on mei-yu precipitation. The spatial distributions of geopotential height and geopotential height anomalies at 500 hPa under different configurations of the EASJ and EAPJ show large differences (Fig. 6). For the SS situation, the WPSH is strong and extends westward to  $122^\circ\text{E}$ . Synoptic circulation in the mid- to high latitude shows a typical ridge–trough–ridge pattern: two positive anomalies appear over the Ural Mountains and Okhotsk Sea, and a negative anomaly exists in between. For the SW situation, the WPSH shifts northward and westward than its normal position. The Okhotsk Sea and Lake Baikal region is controlled by a negative anomaly. For the WS situation, the WPSH shifts eastward to the ocean. Mid- to high-latitude circulation shows a trough–ridge pattern: a negative anomaly exists in Ural Mountains and a positive anomaly appears over the Lake Baikal and Okhotsk Sea. For the WW situation, the WPSH is weak. The mid- to high-latitude region of Asia is controlled by negative anomalies. A positive anomaly appears over northeast China.

The appearance of mid- to high-latitude blocking highs is largely associated with the existence of cold air and shows a positive correlation with precipitation amount (Wang 1992; Li and Ding 2004). In this paper,

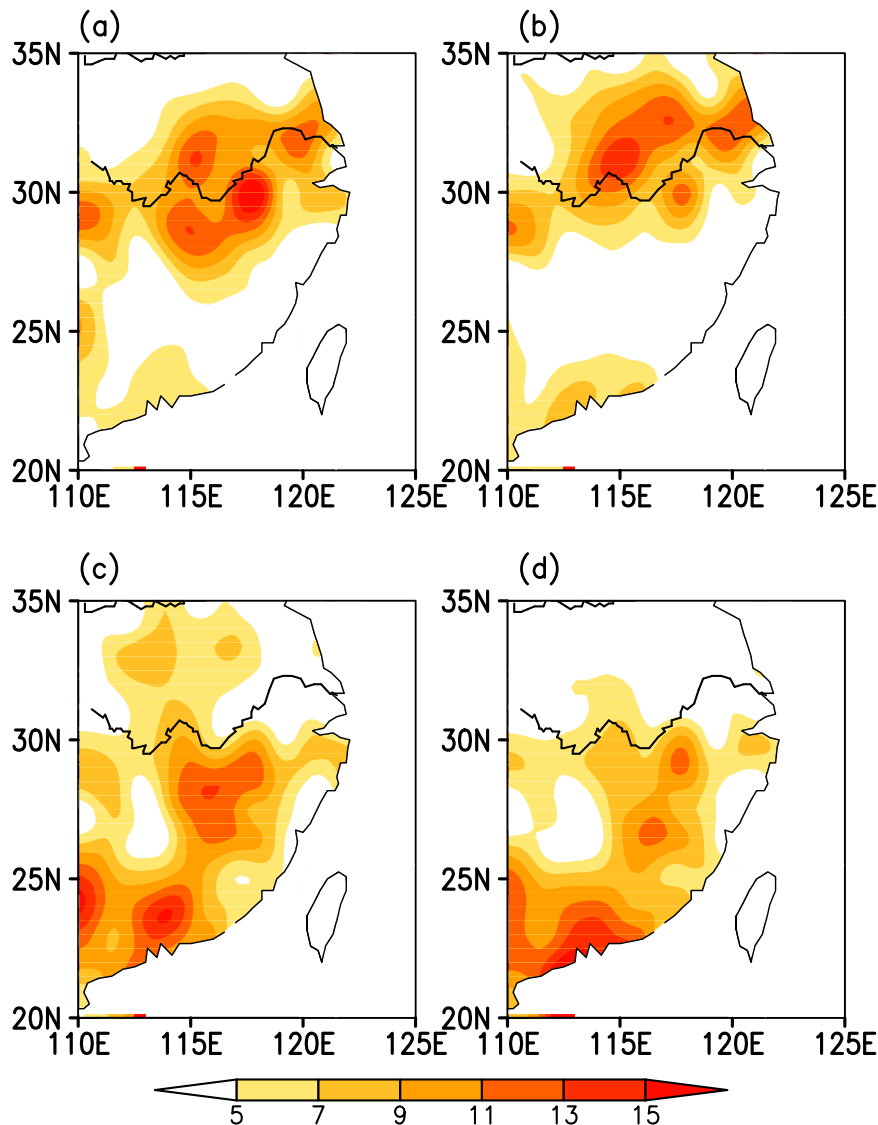


FIG. 5. Spatial distribution of daily precipitation in eastern China ( $\text{mm day}^{-1}$ ) with different configurations of the EASJ and EAPJ: (a) strong EASJ and strong EAPJ, (b) strong EASJ and weak EAPJ, (c) weak EASJ and strong EAPJ, and (d) weak EASJ and weak EAPJ.

the blocking high detection algorithm follows the one adopted by Barriopedro et al. (2006). Blocking high occurrence numbers on different longitude with different configurations of the EASJ and EAPJ are given in Fig. 7. For the SS situation, blocking highs appear most often in  $120^{\circ}\text{--}160^{\circ}\text{E}$  and  $60^{\circ}\text{--}80^{\circ}\text{E}$ . For the SW situation, the occurrence number of blocking high is small. For the WS situation, blocking occurs most frequently in  $120^{\circ}\text{--}160^{\circ}\text{E}$ . For the WW situation, blocking highs mainly located in  $40^{\circ}\text{--}80^{\circ}\text{E}$ . So the different configurations of the EASJ and EAPJ correspond to different circulation patterns in the mid- to high latitude.

In general, the 340-K contour of the pseudo-equivalent potential temperature ( $\theta_{\text{se}}$ ) in 850 hPa can illustrate the northern frontier of the monsoon air mass (Wu 1999). Figure 8 presents the spatial distributions of the 340-K contour of  $\theta_{\text{se}}$  at 850 hPa with different configurations of the EASJ and EAPJ. The 340-K contour of  $\theta_{\text{se}}$  is located farther north for cases under the SW situation, namely the monsoon air mass advances farther north. This is consistent with the location of the mei-yu rainband in Fig. 5b. For the WS cases, the 340-K contour of  $\theta_{\text{se}}$  is in a southern position, corresponding with the strong precipitation in southern YHRB (Fig. 5c).

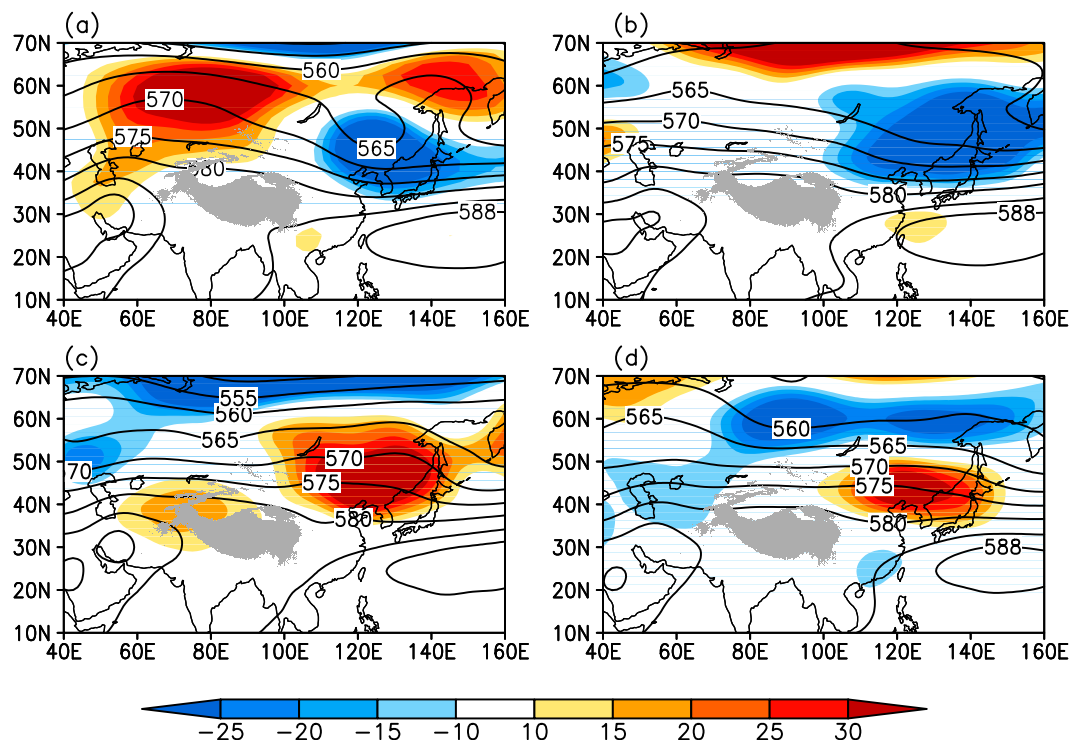


FIG. 6. Spatial distribution of geopotential height (contour) and geopotential height anomalies (shaded) at 500 hPa with different configurations of the EASJ and EAPJ: (a) strong EASJ and strong EAPJ, (b) strong EASJ and weak EAPJ, (c) weak EASJ and strong EAPJ, and (d) weak EASJ and weak EAPJ.

## 6. Warm/cold airmass activities with different configurations of EASJ and EAPJ

Generally speaking, mei-yu precipitation formation is associated with the confluence of warm and cold air masses. Some previous studies have focused on warm and cold airmass activities (Shinoda et al. 2005; Yao and Yu 2005), but no large-scale circulation indicator can be used to quantify the intensities of the warm and cold air masses. In this study, we analyze the relationship between the EASJ and EAPJ and the cold/warm airmass activities. It is found that index SJ and index PJ can reflect the intensities of the warm and cold air masses. We also analyze activities of the cold and warm air masses with different configurations of the EASJ and EAPJ.

To analyze the relationship between the EASJ and warm airmass activity, we select 18 cases in which the intensity of the EASJ varies from weak to strong. Figure 9 shows the changes of the EASJ intensity index (index SJ) with time for the 18 selected cases. The time for a weak EASJ to intensify into a strong one is about 5 days, hence, the time series of daily EASJ intensity index for a 5-day period is plotted in Fig. 9. The activity of a warm air mass in these cases is then examined. Warm airmass activity and its intensity are characterized by 24-h

temperature and specific humidity changes in the low-latitude area. Meridional-vertical cross sections of daily temperature and specific humidity changes averaged from 110° to 120°E for the consecutive 4 days are shown in Fig. 10. On the first day, the warming center is located at about 25°–27°N and the maximum warming value appears in 925 hPa with a temperature rise of about 0.25°C. The humidity increase center is situated in 30°N. At the second day, the warming center is located at 29°–30°N and the maximum value appears in 850 hPa with a temperature increase of about 0.35°C. The humidity increase center is situated in 33°N. On the third day, the warming center moves northward to 31°N with temperature rise of about 0.2°C. The humidity increase center progresses to north of 35°N. At the fourth day, the warming center continues to move northward to 33°N and the maximum value occurs at the ground level with a temperature increase of more than 0.35°C. The humidity increase center is situated in 37°N. The above results indicate that the warm air mass in the lower troposphere advances northward when the EASJ intensifies, the EASJ is closely linked to the activity of the warm air mass.

Twelve cases are selected for the study of relationship between the EAPJ intensity and the cold airmass



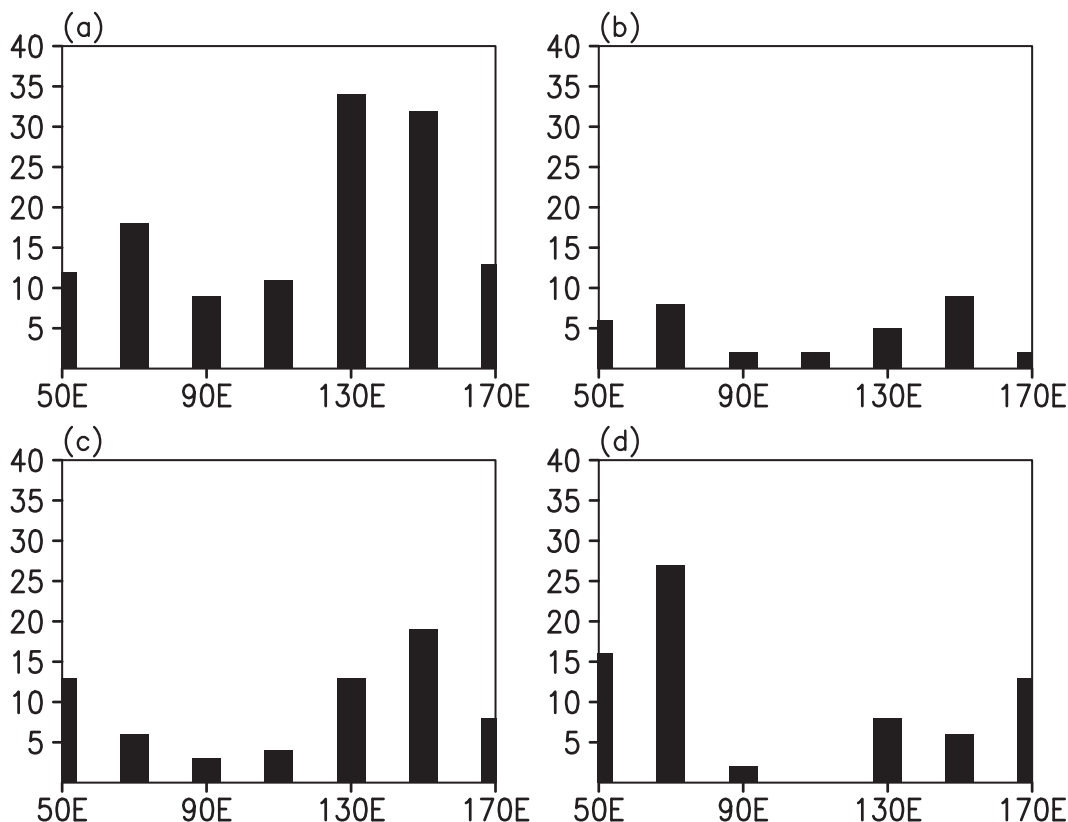


FIG. 7. Blocking high numbers on different longitude with different configurations of the EASJ and EAPJ: (a) strong EASJ and strong EAPJ, (b) strong EASJ and weak EAPJ, (c) weak EASJ and strong EAPJ, and (d) weak EASJ and weak EAPJ.

activity. The intensity of the EAPJ in the 12 cases varies from weak to strong. Figure 11 describes the changes of EAPJ intensity index (index PJ) with time in 12 cases. The process for a weak EAPJ to intensify into a strong one lasts for about 6 days. The activity of the cold air mass in these cases is examined. The 24-h temperature changes in the mid- to high latitude can indicate the activity of the cold air mass. Meridional-vertical cross

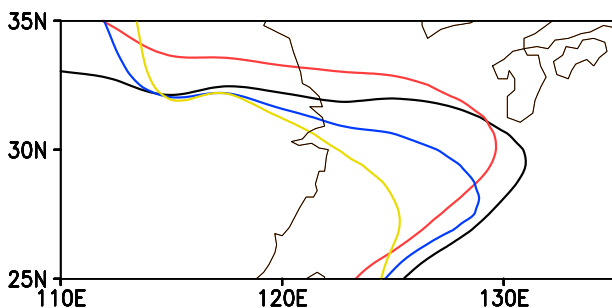


FIG. 8. Spatial distribution of 340-K  $\theta_{se}$  isoline at 850 hPa with different configurations of the EASJ and EAPJ (black line: strong EASJ and strong EAPJ, red line: strong EASJ and weak EAPJ, blue line: weak EASJ and strong EAPJ, and yellow line: weak EASJ and weak EAPJ).

sections of daily temperature changes averaged from 110° to 120°E are shown in Fig. 12. At the first day, the cooling center is located at 55°N, and temperature decreases by about 0.35°C. At the second day, the cooling center is located at 50°N and the maximum

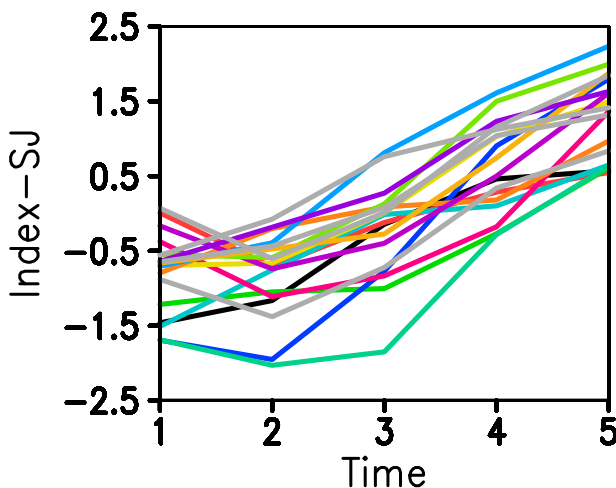


FIG. 9. Eighteen cases of the strength of EASJ changes from weak to strong.

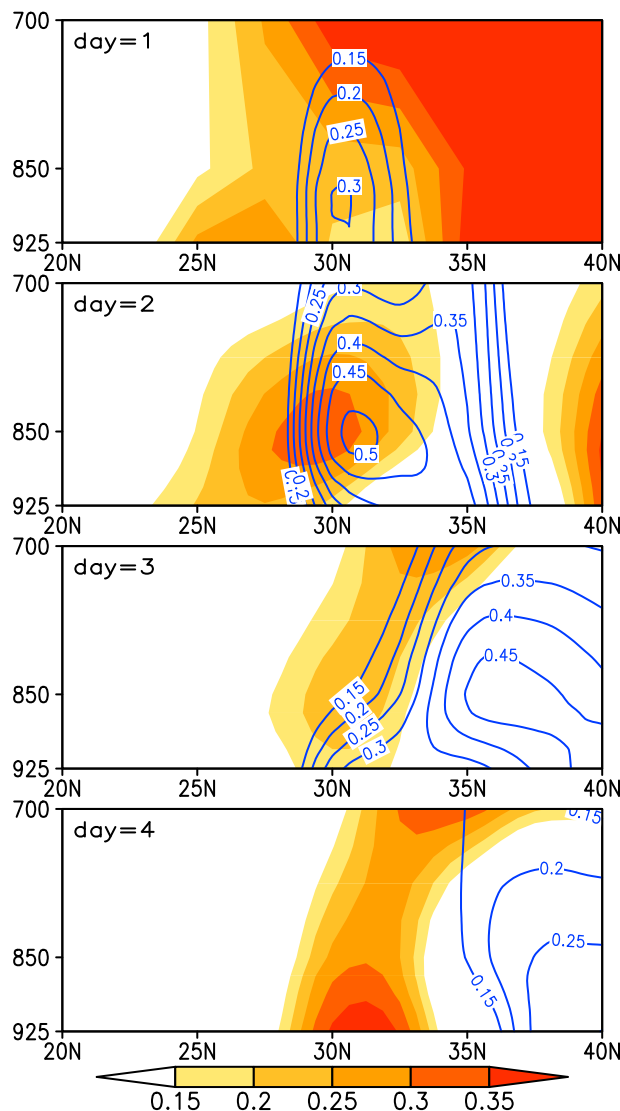


FIG. 10. The temperature difference in 24 h (K, shaded) and specific humidity difference in 24 h ( $10^{-3} \text{ g kg}^{-1}$ , contour) over  $110^{\circ}$ – $120^{\circ}\text{E}$  in the process from weak EASJ to strong EASJ.

cooling occurs at 850 hPa with a temperature decrease of about  $1^{\circ}$ – $1.5^{\circ}\text{C}$ . At the third day, the cooling center moves southward to  $43^{\circ}\text{N}$  and the temperature decreases by about  $1^{\circ}\text{C}$ . At the fourth day, the cooling center continues to move southward to  $40^{\circ}\text{N}$  and finally reaches the YHRB at the fifth day. The above results clearly indicate that the cold air mass in the upper troposphere sinks to lower levels and moves southward with the EAPJ intensification, the EAPJ is linked to the cold air-mass activity.

Further analyses show the activities of warm and cold air masses with different intensity configurations of the EASJ and EAPJ. The day = 0 in Fig. 13, 14, 15 are days that satisfy the definition for strong EASJ and strong

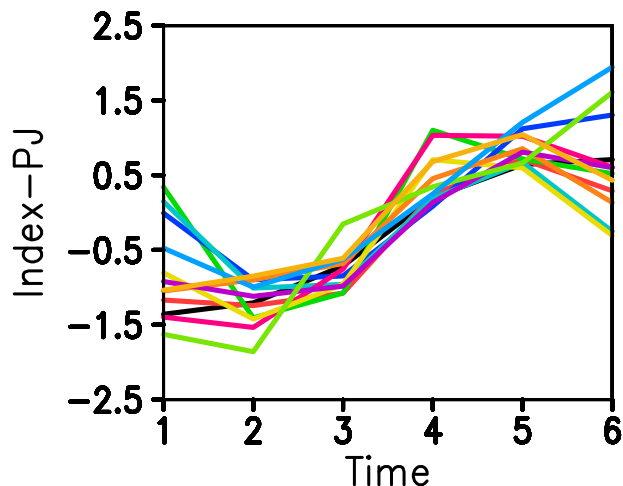


FIG. 11. Twelve cases of the strength of EAPJ changes from weak to strong.

EAPJ, strong EASJ and weak EAPJ, and weak EASJ and strong EAPJ, respectively. The day =  $-n$  are obtained by backward  $n$  days. For the SS cases, both the warm and cold air masses are active. The temperature rises over the  $25^{\circ}$ – $30^{\circ}\text{N}$  in 4 days before the SS cases, and

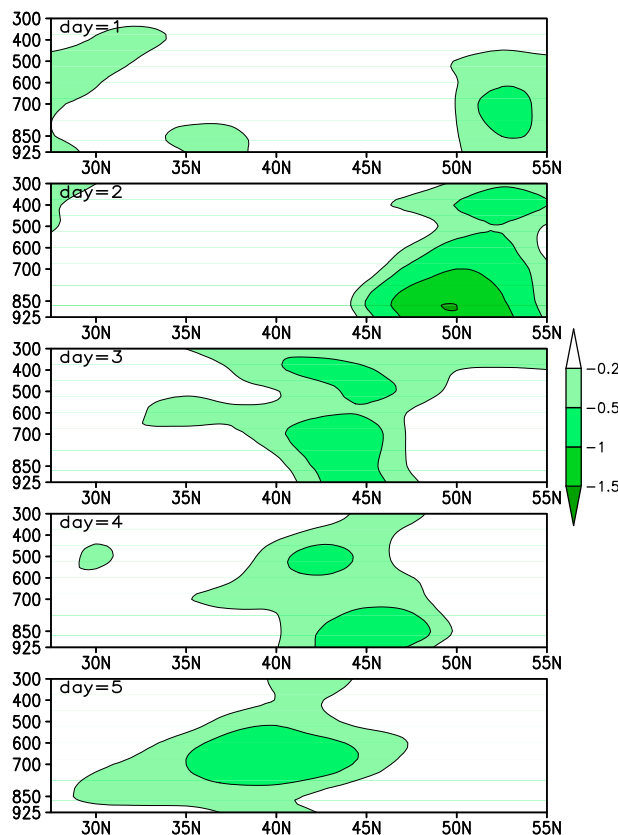


FIG. 12. Temperature difference in 24 h over  $110^{\circ}$ – $120^{\circ}\text{E}$  in the process from weak EAPJ to strong EAPJ.



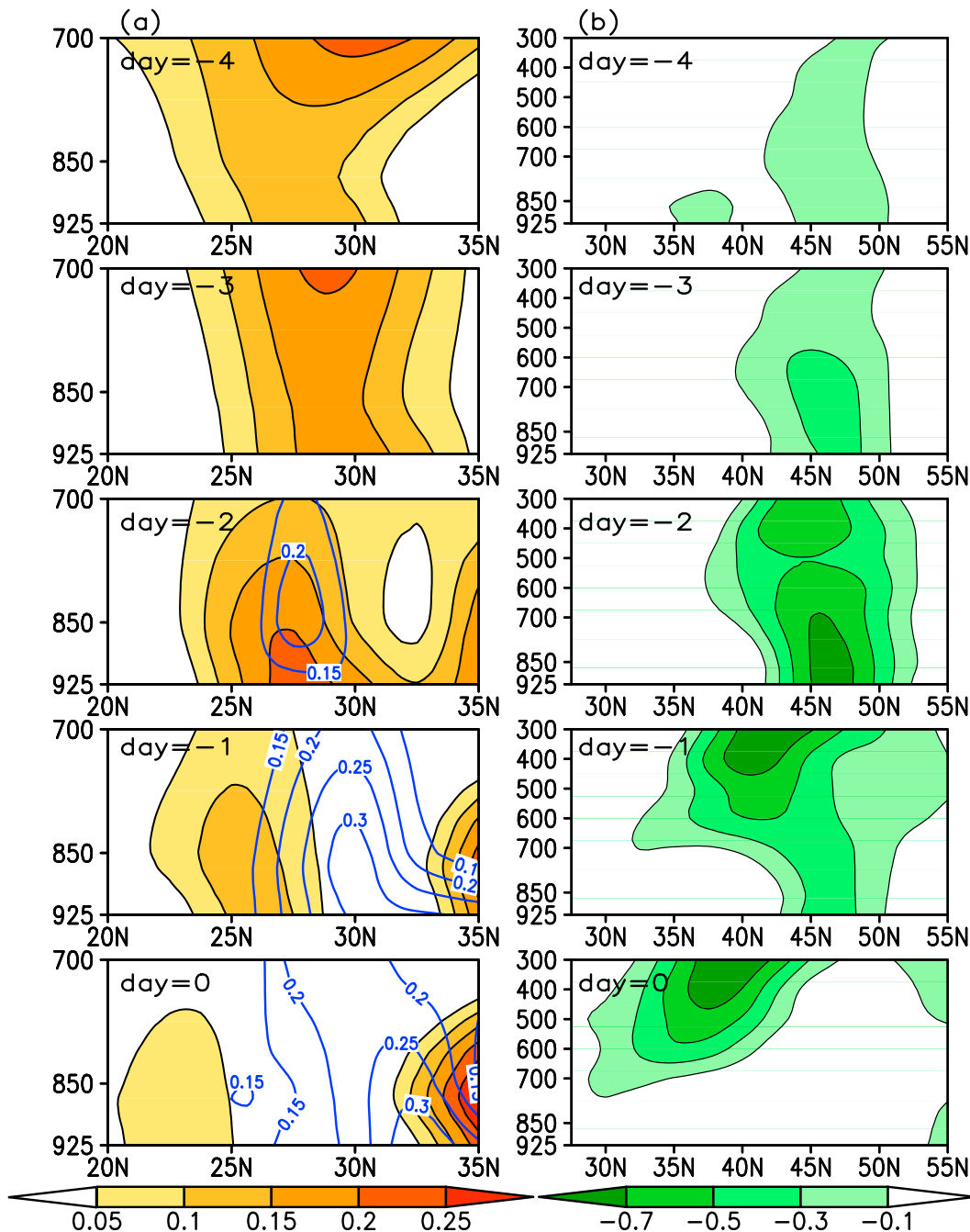


FIG. 13. The activity of (a) warm and (b) cold air masses before strong EASJ and strong EAPJ cases. (blue lines: specific humidity difference in 24 h; shading: temperature difference in 24 h).

the temperature rises by  $0.5^{\circ}\text{C}$  in this region (Fig. 13a), the humidity increased significantly in 2 days before the SS cases. The cold air mass extends southward from  $50^{\circ}$  to  $30^{\circ}\text{N}$  in 4 days before the SS cases (Fig. 13b). The warm and cold air masses meet at nearby  $30^{\circ}\text{N}$ , leading to abundant precipitation in the YHRB (Fig. 5a). At day = 0, the decrease of temperature in  $30^{\circ}\text{N}$  is due to

precipitation. For the SW cases, the warm air mass is stronger than the cold air mass, resulting in northward advancement of the warm air mass. In 4 days before SW cases, the temperature over  $25^{\circ}$ – $33^{\circ}\text{N}$  rises by  $0.8^{\circ}\text{C}$  and humidity is increased significantly over  $33^{\circ}$ – $35^{\circ}\text{N}$  (Fig. 14a); the cold air mass extends southward from  $45^{\circ}$  to  $33^{\circ}\text{N}$  and the maximum cooling area is at around

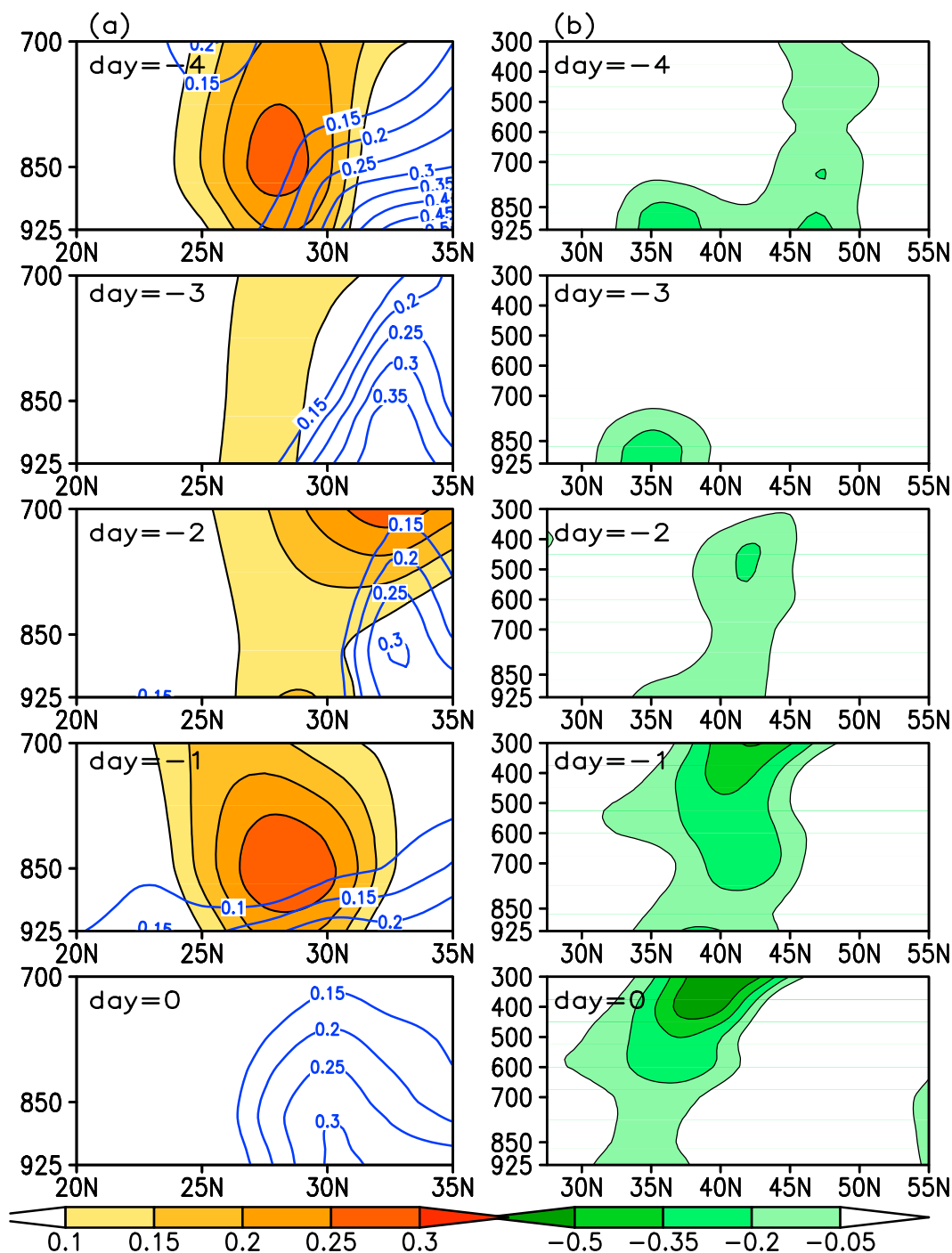


FIG. 14. As in Fig. 13, but for strong EASJ and weak EAPJ.

35°–40°N, where the temperature reduces by 0.6°C (Fig. 14b). The warm air mass meets the cold air mass at about 33°N, leading to heavy precipitation in the north of YHRB (Fig. 5b). For the WS cases, the cold air mass is stronger than the warm air mass, resulting in southward advancement of the cold air mass. The temperature rises over 20°–25°N in four 4 days before the WS

cases (Fig. 15a); the cold air extends southward from 45° to 25°N, the temperature does not drop as large as in the SS cases, but the cold air mass reaches the YHRB more quickly and lasts for a longer time (Fig. 15b). The warm and cold air masses meet near 25°N, and precipitation occurs in the south of YHRB (Fig. 5c).

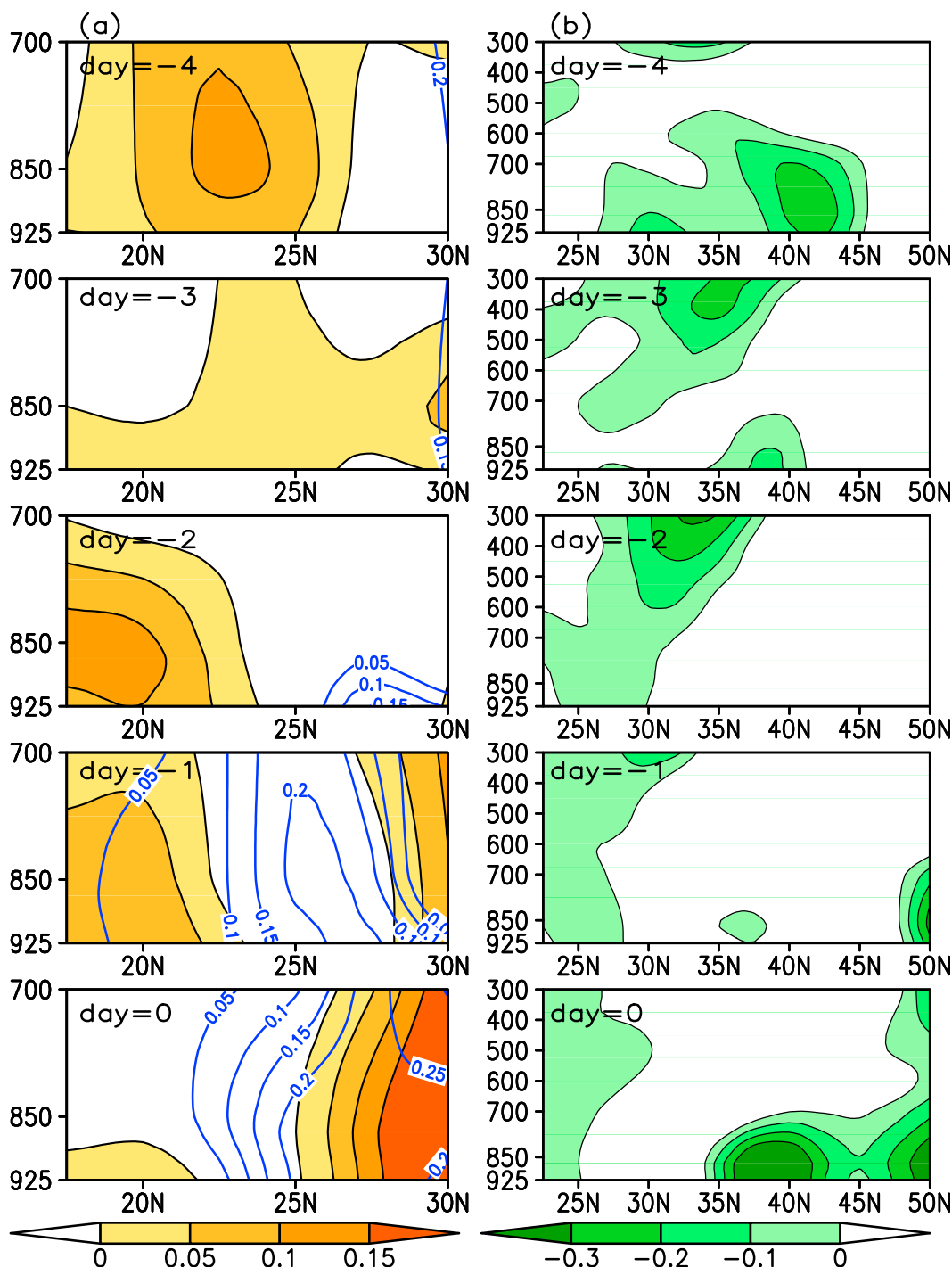


FIG. 15. As in Fig. 13, but for weak EASJ and strong EAPJ.

## 7. Conclusions and discussion

The East Asian jet system consists of two branches: the East Asian subtropical jet (EASJ) and the East Asian polar front jet (EAPJ). This study investigates the effect of different configurations of the EASJ and EAPJ

on precipitation in the YHRB during the mei-yu season. Based on analysis of wind speed and jet center occurrence numbers, the regions of 35°–40°N, 100°–140°E and 62.5°–72.5°N, 80°–140°E are taken as the key areas for assessing the EASJ and EAPJ activities. The daily area average wind speeds at 300 hPa over the key areas are

defined as the daily intensity indices for EASJ and EAPJ. The individual variations of EASJ/ EAPJ and their impacts on precipitation are investigated first. The precipitation intensity increases with enhanced activities of the EASJ and EAPJ. Rainband is located to the northern side of YHRB when the EASJ intensifies and the EAPJ weakens. The effects of concurrent variation of the EASJ and EAPJ on mei-yu precipitation are then analyzed. Based on the configurations of the EASJ and EAPJ intensity, four situations are classified: a strong EASJ with a strong EAPJ (SS), a strong EASJ with a weak EAPJ (SW), a weak EASJ with a strong EAPJ (WS), and a weak EASJ with a weak EAPJ (WW). A number of cases are selected to demonstrate various precipitation features under each of the four situations. For cases under the SS situation, abundant precipitation appears in the YHRB. For cases under the WW situation, no obvious precipitation appears in the YHRB. For cases under the SW situation, precipitation concentrates in the northern YHRB. For WS cases, precipitation mainly occurs at the southern YHRB. The associated circulation analyses indicate that different intensity configurations of the EASJ and EAPJ not only reflect the influence of low-latitude monsoon air mass, but also reflect the impact of mid- to high blocking highs.

Further analyses indicate that the intensity changes of the EASJ and EAPJ are linked with the cold/warm air-mass activities. As the EASJ intensifies, the warm air mass in the lower troposphere advances northward; as the EAPJ intensifies, the cold air mass in the upper troposphere sinks to lower levels and moves southward. The warm and cold airmass activities vary significantly with different configurations of the EASJ and EAPJ. For the SS cases, both the warm and cold air masses are active and with similar intensity variation. The warm and cold air masses meet at nearby 30°N, resulting in heavy precipitation there. For the WW cases, both the warm and cold air masses are inactive, and no significant precipitation occurs in the YHRB. For the SW cases, the warm air mass advances farther north while the cold air mass is weak. For the WS cases, the cold air mass extends southward while the warm air mass is weak.

Compared with the individual variation of EASJ, the concurrent variation between the two jets not only reflects the influence of low-latitude circulation systems, but also reflects the impact of the mid- to high-latitude circulation system, so it better reflect the upper-level circulation systems and mei-yu precipitation distribution. The results partly reveal the mechanisms responsible for the effects of different configurations of the EASJ and EAPJ on mei-yu precipitation, which still need further study in the future. In addition, the East Asian jet system varies at multiple time scales. The previous study by Liao and Zhang (2013) suggested that the interaction between the EASJ and

EAPJ has an important influence on winter weather at the intraseasonal scale. During the mei-yu season, persistent heavy rainfall is the most important weather phenomenon in summer. Impacts of the EASJ and EAPJ on the persistent heavy rainfall events will also be investigated in our future study. Moreover, the results obtained in our study are only base on NCEP1 data. Recent comparisons of multireanalysis data over global monsoon and Tibetan Plateau domains found some differences (Feng and Zhou 2012; Lin et al. 2014), so comparisons between different datasets are also needed in future work.

**Acknowledgments.** The authors thank the editor and three anonymous reviewers who provided valuable suggestions for improving our manuscript. This work was jointly supported by the National Natural Science Foundation of China (Grant 41130963), the National Basic Research Program of China (973 Program, Grant 2012CB955901), China Meteorological Administration Special Public Welfare Research Fund (GYHY201006019), and the Jiangsu Collaborative Innovation Center for Climate Change.

## REFERENCES

- Akiyama, T., 1973: The large-scale aspects of the characteristic features of the Baiu front. *Pap. Meteor. Geophys.*, **24** (2), 157–188.
- Ambrizzi, T., B. J. Hoskins, and H.-H. Hsu, 1995: Rossby wave propagation and teleconnection patterns in the austral winter. *J. Atmos. Sci.*, **52**, 3661–3672, doi:10.1175/1520-0469(1995)052<3661:RWPATP>2.0.CO;2.
- Barriopedro, D., R. García-Herrera, A. R. Lupo, and E. Hernández, 2006: A climatology of Northern Hemisphere blocking. *J. Climate*, **19**, 1042–1063, doi:10.1175/JCLI3678.1.
- Chang, C.-P., Ed., 2004: *East Asian Monsoon*. World Scientific, 564 pp.
- Chen, G.-S., R.-H. Huang, and L.-T. Zhou, 2013: Baroclinic instability of the Silk Road pattern induced by thermal damping. *J. Atmos. Sci.*, **70**, 2875–2893, doi:10.1175/JAS-D-12-0326.1.
- Chen, T.-J. G., and C.-P. Chang, 1980: The structure and vorticity budget of an early summer monsoon trough (mei-yu) over southeastern China and Japan. *Mon. Wea. Rev.*, **108**, 942–953, doi:10.1175/1520-0493(1980)108<0942:TSABVO>2.0.CO;2.
- , and C.-C. Yu, 1988: Study of low-level jet and extremely heavy precipitation over northern Taiwan in the mei-yu season. *Mon. Wea. Rev.*, **116**, 884–891, doi:10.1175/1520-0493(1988)116<0884:SOLLJA>2.0.CO;2.
- Ding, Q.-H., and B. Wang, 2005: Circumglobal teleconnection in the Northern Hemisphere summer. *J. Climate*, **18**, 3483–3505, doi:10.1175/JCLI3473.1.
- Ding, Y.-H., 1992: Summer monsoon precipitations in China. *J. Meteor. Soc. Japan*, **70**, 373–396.
- Du, Y., Y.-C. Zhang, and Z.-Q. Xie, 2008: Impacts of longitude location changes of East Asian westerly jet core on the precipitation distribution during Mei-yu period in middle-lower reaches of Yangtze River valley. *Acta Meteor. Sin.*, **66**, 566–576.
- Enomoto, T., 2004: Interannual variability of the Bonin high associated with the propagation of Rossby waves along the Asian jet. *J. Meteor. Soc. Japan*, **82**, 1019–1034, doi:10.2151/jmsj.2004.1019.

- Feng, L., and T.-J. Zhou, 2012: Water vapor transport for summer precipitation over the Tibetan Plateau: Multidataset analysis. *J. Geophys. Res.*, **117**, D20114, doi:[10.1029/2011JD017012](https://doi.org/10.1029/2011JD017012).
- Gong, D.-Y., and C.-H. Ho, 2003: Arctic oscillation signals in the East Asian summer monsoon. *J. Geophys. Res.*, **108**, 4066, doi:[10.1029/2002JD002193](https://doi.org/10.1029/2002JD002193).
- , S.-W. Wang, and J.-H. Zhu, 2001: East Asian winter monsoon and Arctic oscillation. *Geophys. Res. Lett.*, **28**, 2073–2076, doi:[10.1029/2000GL012311](https://doi.org/10.1029/2000GL012311).
- Hoskins, B. J., and T. Ambrizzi, 1993: Rossby wave propagation on a realistic longitudinally varying flow. *J. Atmos. Sci.*, **50**, 1661–1671, doi:[10.1175/1520-0469\(1993\)050<1661:RWPOAR>2.0.CO;2](https://doi.org/10.1175/1520-0469(1993)050<1661:RWPOAR>2.0.CO;2).
- Huang, D.-Q., T. Masaaki, and Y.-C. Zhang, 2011: Analysis of the Baiu precipitation and associated circulations simulated by the MIROC coupled climate system model. *J. Meteor. Soc. Japan*, **89**, 625–636, doi:[10.2151/jmsj.2011-603](https://doi.org/10.2151/jmsj.2011-603).
- Kalnay, E., and Coauthors, 1996: The NCEP/NCAR 40-Year Reanalysis Project. *Bull. Amer. Meteor. Soc.*, **77**, 437–471, doi:[10.1175/1520-0477\(1996\)077<0437:TNYRP>2.0.CO;2](https://doi.org/10.1175/1520-0477(1996)077<0437:TNYRP>2.0.CO;2).
- Kodama, Y. M., 1992: Large-scale common features of subtropical precipitation zones (the Baiu frontal zone, the SPCZ, and the SACZ). Part I: Characteristics of subtropical frontal zones. *J. Meteor. Soc. Japan*, **70**, 813–836.
- Kuang, X.-Y., and Y.-C. Zhang, 2006: Impact of the position abnormalities of East Asian subtropical westerly jet on summer precipitation in middle-lower reaches of Yangtze River. *Plateau Meteor.*, **25**, 382–389.
- Lau, K.-M., G.-J. Yang, and S.-H. Shen, 1988: Seasonal and intraseasonal climatology of summer monsoon precipitation over East Asia. *Mon. Wea. Rev.*, **116**, 18–37, doi:[10.1175/1520-0493\(1988\)116<0018:SAICOS>2.0.CO;2](https://doi.org/10.1175/1520-0493(1988)116<0018:SAICOS>2.0.CO;2).
- , K. M. Kim, and S. Yang, 2000: Dynamical and boundary forcing characteristics of regional components of the Asian summer monsoon. *J. Climate*, **13**, 2461–2482, doi:[10.1175/1520-0442\(2000\)013<2461:DABFCO>2.0.CO;2](https://doi.org/10.1175/1520-0442(2000)013<2461:DABFCO>2.0.CO;2).
- Lee, S., and H. K. Kim, 2003: The dynamical relationship between subtropical and eddy-driven jets. *J. Atmos. Sci.*, **60**, 1490–1503, doi:[10.1175/1520-0469\(2003\)060<1490:TDRBSA>2.0.CO;2](https://doi.org/10.1175/1520-0469(2003)060<1490:TDRBSA>2.0.CO;2).
- Li, C.-Y., J.-T. Wang, S.-Z. Lin, and H. Cho, 2004: The relationship between east Asian summer monsoon activity and northward jump of the upper westerly jet location. *Chin. J. Atmos. Sci.*, **28**, 641–658.
- Li, F., and Y. H. Ding, 2004: Statistical characteristic of atmospheric blocking in the Eurasia high-mid latitudes based on recent 30-year summers. *Acta Meteor. Sin.*, **62**, 347–354.
- Liao, Z.-J., and Y.-C. Zhang, 2013: Concurrent variation between the East Asian subtropical jet and polar front jet during persistent snowstorm period in 2008 winter over southern China. *J. Geophys. Res. Atmos.*, **118**, 6360–6373, doi:[10.1002/jgrd.50558](https://doi.org/10.1002/jgrd.50558).
- Lin, R.-P., T.-J. Zhou, and Y. Qian, 2014: Evaluation of global monsoon precipitation changes based on five reanalysis datasets. *J. Climate*, **27**, 1271–1289, doi:[10.1175/JCLI-D-13-00215.1](https://doi.org/10.1175/JCLI-D-13-00215.1).
- Lin, Z.-D., and R.-Y. Lu, 2008: Abrupt northward jump of East Asian upper-tropospheric jet stream in mid-summer. *J. Meteor. Soc. Japan*, **86**, 857–866, doi:[10.2151/jmsj.86.857](https://doi.org/10.2151/jmsj.86.857).
- Lu, R.-Y., 2004: Associations among the components of the East Asian summer monsoon system in the meridional direction. *J. Meteor. Soc. Japan*, **82**, 155–165, doi:[10.2151/jmsj.82.155](https://doi.org/10.2151/jmsj.82.155).
- , J.-H. Oh, and B.-J. Kim, 2002: A teleconnection pattern in upper-level meridional wind over the North African and Eurasian continent in summer. *Tellus*, **54A**, 44–55, doi:[10.1034/j.1600-0870.2002.00248.x](https://doi.org/10.1034/j.1600-0870.2002.00248.x).
- Ninomiya, K., and H. Muraki, 1986: Large-scale circulations over East Asia during Baiu period of 1979. *J. Meteor. Soc. Japan*, **64**, 409–429.
- Ren, X.-J., X.-Q. Yang, and C.-J. Chu, 2010: Seasonal variations of the synoptic-scale transient eddy activity and polar front jet over East Asia. *J. Climate*, **23**, 3222–3233, doi:[10.1175/2009JCLI3225.1](https://doi.org/10.1175/2009JCLI3225.1).
- , —, T.-J. Zhou, and J. Fang, 2011: Diagnostic comparison of wintertime East Asian subtropical jet and polar-front jet: Large-scale characteristics and transient eddy activities. *Acta Meteor. Sin.*, **25**, 21–33, doi:[10.1007/s13351-011-0002-2](https://doi.org/10.1007/s13351-011-0002-2).
- Sampe, T., and S.-P. Xie, 2010: Large-scale dynamics of the meiyu-baiu rainband: Environmental forcing by the westerly jet. *J. Climate*, **23**, 113–134, doi:[10.1175/2009JCLI3128.1](https://doi.org/10.1175/2009JCLI3128.1).
- Shinoda, T., H. Uyeda, and K. Yoshimura, 2005: Structure of moist layer and sources of water over the southern region far from the Meiyu/Baiu front. *J. Meteor. Soc. Japan*, **83**, 137–152, doi:[10.2151/jmsj.83.137](https://doi.org/10.2151/jmsj.83.137).
- Tao, S.-Y., and L.-X. Chen, 1987: A review of recent research on the East Asia summer monsoon in China. *Monsoon Meteorology*, C. P. Chang and T. N. Krishnamurti, Eds., Oxford University Press, 60–92.
- Wang, W.-Z., Z.-C. Zhao, D.-Y. Gong, and T.-J. Zhou, 2005: *Introduction of Climatology*. China Meteorological Press, 43 pp.
- Wang, Y., 1992: Effects of blocking anticyclones in Eurasia in the rainy season (Meiyu/Baiu season). *J. Meteor. Soc. Japan*, **70**, 929–951.
- Wu, R.-S., Ed., 1999: *Principles of Modern Weather*. Higher Education Press, 214 pp.
- Xuan, S.-L., Q.-Y. Zhang, and S.-Q. Sun, 2011: Anomalous mid-summer rainfall in Yangtze River-Huaihe River valleys and its association with the East Asia westerly jet. *Adv. Atmos. Sci.*, **28**, 387–397, doi:[10.1007/s00376-010-0111-3](https://doi.org/10.1007/s00376-010-0111-3).
- Yang, S., K.-M. Lau, and K. M. Kim, 2002: Variations of the East Asian jet stream and Asian-Pacific–American winter climate anomalies. *J. Climate*, **15**, 306–325, doi:[10.1175/1520-0442\(2002\)015<0306:VOTEAJ>2.0.CO;2](https://doi.org/10.1175/1520-0442(2002)015<0306:VOTEAJ>2.0.CO;2).
- Yao, X.-P., and Y.-B. Yu, 2005: Activity of dry cold air and its impacts on Meiyu rain during 2003 Meiyu period. *Chin. J. Atmos. Sci.*, **29**, 973–985.
- Yasui, S., and M. Watanabe, 2010: Forcing processes of the summertime circumglobal teleconnection pattern in a dry AGCM. *J. Climate*, **23**, 2093–2114, doi:[10.1175/2009JCLI3323.1](https://doi.org/10.1175/2009JCLI3323.1).
- Ye, D.-Z., S.-Y. Tao, and M.-C. Li, 1958: The abrupt change of circulation over Northern Hemisphere during June and October (in Chinese). *Acta Meteor. Sin.*, **29**, 249–263.
- Zhang, L.-X., and T.-J. Zhou, 2012: The interannual variability of summer upper-tropospheric temperature over East Asia. *J. Climate*, **25**, 6539–6553, doi:[10.1175/JCLI-D-11-00583.1](https://doi.org/10.1175/JCLI-D-11-00583.1).
- Zhang, Y.-C., and C.-L. Xiao, 2013: Variability modes of the winter upper-level wind field over Asian mid-high latitude region. *Atmos. Oceanic Sci. Lett.*, **6**, 295–299.
- , X.-Y. Kuang, W.-D. Guo, and T. Zhou, 2006: Seasonal evolution of the upper-tropospheric westerly jet core over East Asia. *Geophys. Res. Lett.*, **33**, L11708, doi:[10.1029/2006GL026377](https://doi.org/10.1029/2006GL026377).
- , D.-Q. Wang, and X.-J. Ren, 2008: Seasonal variation of the meridional wind in temperate jet stream and its relationship to the Asian monsoon. *Acta Meteor. Sin.*, **22** (4), 446–454.
- Zhou, T.-J., D.-Y. Gong, J. Li, and B. Li, 2009: Detecting and understanding the multi-decadal variability of the East Asian summer monsoon—Recent progress and state of affairs. *Meteor. Z.*, **18**, 455–467, doi:[10.1127/0941-2948/2009/0396](https://doi.org/10.1127/0941-2948/2009/0396).